# SINUSOIDAL VIBRATION MEASUREMENTS IN A PIEZOELECTRIC XY NANOPOSITIONER BY USING A NEW INTERFEROMETRIC METHOD

**Andryos da Silva Lemes**
**José Henrique Galeti**
**Ricardo Tokio Higuti**
**Cláudio Kitano**
Faculdade de Engenharia de Ilha Solteira, UNESP - Universidade Estadual Paulista, Department of Electrical Engineering,
Av. Brasil, 56, 15385-000 – Ilha Solteira, SP, Brazil
andryos.lemes@aluno.feis.unesp.br, jhgaleti@gmail.com, tokio@dee.feis.unesp.br, kitano@dee.feis.unesp.br

**Ronny Calixto Carbonari**
Universidade Federal do ABC, Centro de Engenharia, Modelagem e Ciências Sociais Aplicadas, Rua Santa Adélia, 166,
09210-170 - Santo André, SP – Brazil
ronny.carbonari@ufabc.edu.br

**Emílio Carlos Nelli Silva**
Department of Mechatronics and Mechanical Systems Engineering - Escola Politécnica da Universidade de São Paulo – EPUSP,
Av. Prof. Mello Moraes, 2231, 05508-900 – São Paulo, SP, Brazil
ecnsilva@usp.br

***Abstract.*** *Nanopositioning systems are fundamental in scanning probe microscopy and in microelectronics, where elements with nanometer dimensions are manipulated. These systems require positioning stages with nanoscale resolution for assembly, testing and characterization. It is recognized that piezoelectric actuators are ubiquitous tools in a wide variety of applications, particularly those involving nanomanipulation. A multi-actuated piezoelectric actuator is a device with small dimensions that can be driven by reduced voltages and can produce nanoscale displacements. These devices consist in a multi-flexible structure actuated by two or more piezoceramics. Such structure acts as a mechanical transformer by amplifying and changing the direction of the piezoceramic displacements. In this work, a XY nanopositioner, designed by using the topology optimization technique, is tested. Measurements of nanodisplacements require calibration by comparison with an absolute standard, and this is performed by using interferometers. A low cost homodyne Michelson interferometer is used to detect the nanovibrations of XY actuators, using a method based on the spectral analysis of the photodetected signal. This new method is self-consistent, is immune to fading, does not demand Bessel functions algebraic sign correction algorithms, does not present singularities when the static phase shift between the interferometer arms is equal to an integer multiple of $\pi/2$ rad, and has a wide dynamic range (from 0.18 to 130 rad). The XY nanopositioner characterization was based on the determination of the actuator length-to-voltage sensitivities (in nm/V), displacement frequency response and coupling rate between the generated and coupled displacements.*

***Keywords:*** *nanopositioner XY, nanometric displacement, laser interferometry, PZT*

## 1. INTRODUCTION

Nowadays there is a substantial interest in multi-actuated piezoelectric actuators (MAPFAs), which are solid state mechanisms where the action is given by the structural flexibility and not by the presence of joints and pins (Carbonari et al., 2005a). They are assembled in a single part and can also amplify and change the direction of piezoceramic displacements. New MAPFAs models have been developed using the topology optimization technique, which is a method of computational design that combines an optimization algorithm and finite element method (FEM) to obtain the optimal topology of the mechanical parts.

The design of a MAPFA must take into account the displacement amplification provided by the flexible structure and the force produced in the desired displacement direction. These parameters can be optimized if the structure is designed to provide flexibility and stiffness. Numerical analysis with ANSYS software is used to model the devices, taking into consideration all structure components: piezoceramics, adhesives, excitation type, clamped points, etc. The goal of topology optimization is to determine, through the addition and removal of material, a continuous solid structure that meets the specified objective function (Carbonari et al., 2007).

One potential application of MAPFAs is in the area of nanotechnology, which deals with objects whose size is below 100 nm and thus below atomic scale dimensions (Zhelkobaev et al., 2007). The micro/nano manufacturing is an emerging industry with significant market potential, but the available measurement tools are still complicated. Scanning probe microscopy (SPM) has become the main technique for characterization, nanomechanical testing and nanoassembly, and atomic force microscopy (AFM) is the most frequently used SPM. These systems require

positioning mechanisms with nanoscale resolution and, consequently, fundamental issues in nanotechnology and future advances in the field of SPM depend on stages of nano positioning with high resolution and high bandwidth (Devasia et al., 2007).

It is well known that accuracy and resolution positioning of manipulators depend mainly on their topological and mechanical structures, which should preferably be flexure-based mechanisms (Tian et al., 2009). Thus, over the years, various arrangements have been proposed for nanometric positioners as, for example, the multi-actuated microtools (Carbonari et al., 2007; Carbonari et al., 2005a) (as the MPFAs in this paper), the multi-actuated functionally graded piezoelectric micro-tools (Carbonari et al., 2009), the flexure based hexapod nanopositioner (Shi et al., 2013), the KoalaDrive nanopositioner (Cherepanov et al., 2012), the flexure-based five bar mechanism (Tian et al., 2009) and many others (Devasia et al., 2007).

This suggests that the measurement of very small displacements with high accuracies is the foundation for a variety of applications in nanotechnology, such as, for calibration of STM and AFM, holographic scales and many other actuator types (Schibli et al., 2006). The interferometers are often used in nanopositioning devices and nanomeasurements because use frequency stabilized lasers and the measurement is traceable to the meter definition and national and international standards (Hausotte et al., 2012).

At the moment, another fundamental and dramatically evolving technology is microelectronics, where elements down to nanometer dimensions are manipulated (Novikov et al., 2007). In this case and, in particular, in very large scale integration (VLSI), there is the challenge of system integration and manipulation over multiple scales, involving several orders of magnitude. All known displacement measurement principles, with a resolution of approximately 1 nm or less, are limited to a very small measurement range (Brand and Herrmann, 1996). Consequently, in nanotechnology, multiscale exploration remains a major challenge (Chassagne et al., 2010). In a multiscale positioning system, the measurement of displacement with high accuracy is of most importance (Kuo et al., 2007), and among the several techniques, optical interferometry are broadly employed, due to simplicity and high sensitivity.

However, despite of being essential in MAPFAs design, compliant mechanisms produce an undesired effect: the displacement in a direction (generated displacement) results in a spurious displacement (coupled displacement) in the other direction. Consequently, measurements of displacement of such structures are of great importance to verify analytical and FEM models, to access the material and device properties, to detect defects and to determine MAPFA performance. Optical techniques, such as the interferometric one, provide several advantages relative to other conventional methods for validating, testing and characterizing MAPFAs.

Finally, because the MAPFAs discussed in this work were developed for static or quasi-static practical applications, far from mechanical resonances, their resonant frequencies must be high enough to guarantee linear operation of the transducers in a wide range of low frequencies and small time response. As the first resonance frequency usually is not considered in their numerical design procedures, interferometry plays an important role in the measurement of these resonance frequencies, bandwidth, linearity, and coupling rate.

There is a general agreement that heterodyne interferometry techniques, with picometer resolution, are useful when the displacement exceeds an interference fringe, while homodyne techniques are often employed when the displacement does not exceed the fringe spacing (Smith et al., 2009). However, homodyne interferometers still have interesting characteristics, such as ease of use, low cost and small periodic error level, which are much more pronounced in heterodyne interferometers (Fan et al., 2007). Moreover, with the availability of inexpensive processing power, some computational signal processing complexity is often preferable to recover the optical path length from the measured photocurrent, instead of additional optics and electronics that are required by other techniques.

In this work, a low cost open-loop homodyne Michelson interferometer is utilized to experimentally detect the nanovibrations of MAPFAs, based on the spectral analysis of the interferometric signal. Based on the well-known $J_1/J_3$ phase demodulation method (Deferrari et al., 1967), a new and improved version is proposed, which presents the following characteristics: is self-consistent, is immune to fading, does not present phase ambiguity problems and presents a wide phase demodulation dynamic range. Modulation indexes values up to 130 rad have been measured with high accuracy, and this limit is determined only by the detector and data acquisition bandwidths employed. This range is sufficient to analyze the MAPFAs discussed in section 2.

## 2. MULTI-ACTUATED PIEZOELECTRIC FLEXTENSIONAL ACTUATORS

Topology optimization is a powerful structural optimization technique that combines the FEM with an optimization algorithm to find the optimal material distribution inside a given domain bounded by supports and applied loads that must contain the unknown structure (Carbonari et al., 2009). The objective of topology optimization is to determine the holes and connectivities of the structure by adding and removing material in the extended fixed domain. The main question to be addressed in topology optimization is how to change the material from zero (void) to one (material). Since piezoelectric actuators are usually two dimensional (2D) devices, the examples presented herein are limited to two dimensions (2D plane stress).

Thus, the development of MAPFA mechanisms requires the design of actuated compliant mechanisms that can perform complex movements. In addition, when multiple piezoceramic devices are involved, coupling effects in their

movements become critical, especially the appearance of undesired movements, which makes the design task very complex. One way to avoid undesirable coupling effects is to use a systematic design method, such as topology optimization, with appropriate formulation of the optimization problem (Carbonari et al., 2005a). Essentially, the optimization problem is posed as the design of a flexible structure that maximizes different output displacements or output forces in different specified directions and points of the domain, in response to different excited piezoceramic portions, with particular attention to minimizing the effects of movement coupling. The MAPFAs considered here operate in quasi-static or low-frequency applications, that is, lower than their first resonance frequency, and so, the inertia effects are neglected (Carbonari et al., 2009).

Figure 2 illustrates the various stages involved in the topology optimization procedure to design a MAPFA (Carbonari et al., 2009). First, an initial design domain is defined [Fig. 2a)], which is limited by the device boundary conditions such as regions where there are restraints and applied loads. This domain is discretized into finite elements [Fig. 2b)] and it is an input to the topology optimization software. The objective of topology optimization is to determine the voids and connectivities of the structure by adding and removing material in the extended fixed domain [Fig. 2c)]. The finite element model domain is not changed during the optimization process. The software gives as a result an optimized material distribution in the design domain, which must be interpreted [Fig. 2d)], verified [Fig. 2e)], and manufactured [Fig. 2f)]. By changing coupling structure topologies, novel designs of flextensional actuators are obtained for different applications. A detailed review of modeling for displacement amplified piezoelectric actuators, the FEM using ANSYS, and their application to compliant mechanism design is given in (Carbonari et al., 2005a; Carbonari et al., 2007, Carbonari et al., 2009).

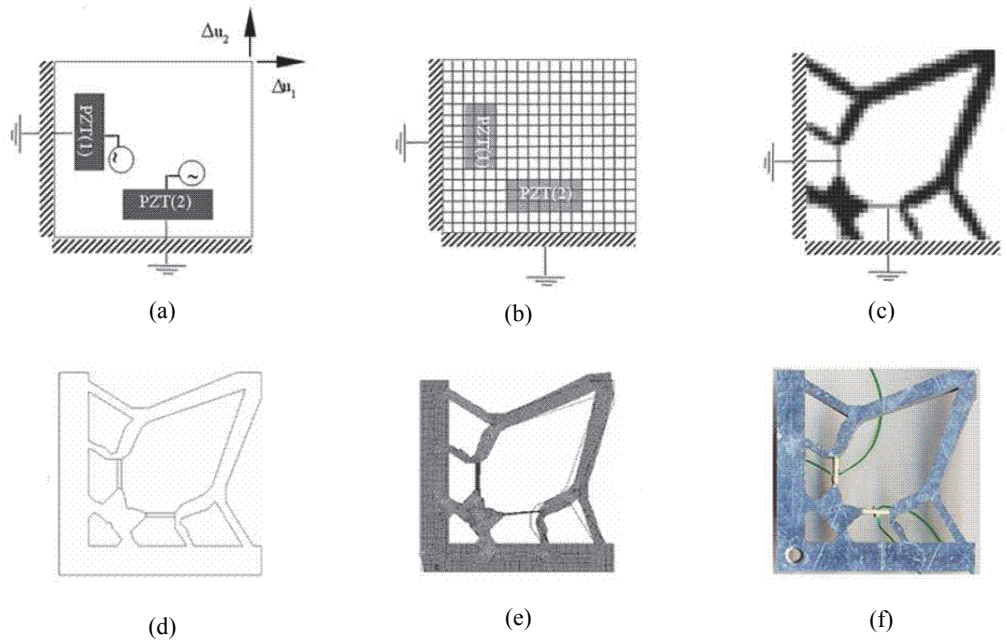


Figure 1. Topology optimization procedure for designing piezoelectric mechanisms (Δu is the desired output displacement) (Carbonari et al., 2009). a) Initial domain, b) Domain discretized, c) Topology obtained, d) Interpretation, e) Verification, and f) Manufactured.

The piezoelectric multi-actuator used in this work consists in a coupling structure actuated by two piezoceramics where each piezoceramic is responsible for actuating a specific multi-actuator movement. In addition, there is a coupling between actuated displacements due to the fact that it is a flexible structure. Thus, when a piezoceramic is excited to generate a desired displacement, other undesired displacements may also be generated. Figure 2 illustrates the MAPFA prototype tested in this work, which uses two piezoceramics (PZT-5A 20 mm x 5 mm x 1 mm in directions 1, 2 and 3, respectively) and an aluminum flexible structure manufactured using a wire EDM (Electrical Discharge Machining) machine. These piezoceramics are polarized in the 3-direction and the electrode surfaces are normal to this direction. Displacement measurement was performed under mechanically 'free' condition. The experiment was performed in air.

Experimental displacement measurements were performed to evaluate the prototype performances in terms of movement generated and coupled displacements. Since these devices are used in static or quasi-static mode, displacements are determined by considering low excitation frequencies. In general, the XY actuator is build to achieve the maximum displacement in X and Y direction with minimum crosstalk between both directions.

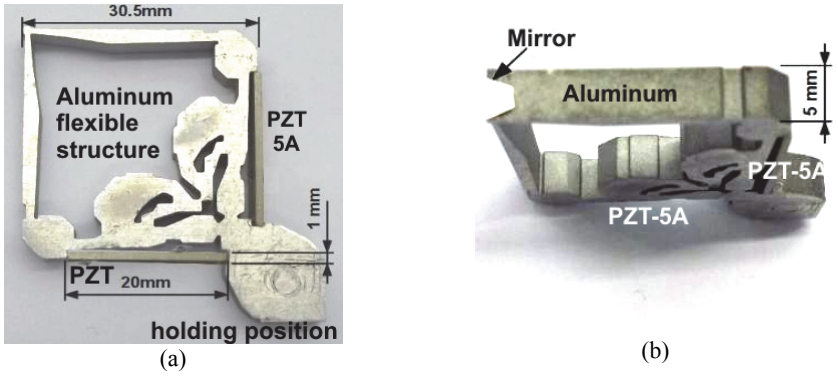


(a) (b)

Figure 2. XY nanopositioner prototype. a) Lateral view. b) Top view.

## 3. OPTICAL INTERFEROMETRY AND CLASSICAL $J_1/J_3$ METHOD

In this work, the experiment is based on a bulk homodyne Michelson interferometer (Udd and Spillman, 2011). Figure 3 shows the schematic of the experimental setup. The laser source is a linearly polarized He-Ne laser. A 50% beam splitter divides the beam into two equal parts. One (the reference beam) is sent to a fixed mirror; the second (the measurement beam) is sent to the MAPFA surface. The back reflected beam is superimposed to that coming from the fixed mirror on the beam-splitter and is sent to the detection assembly.

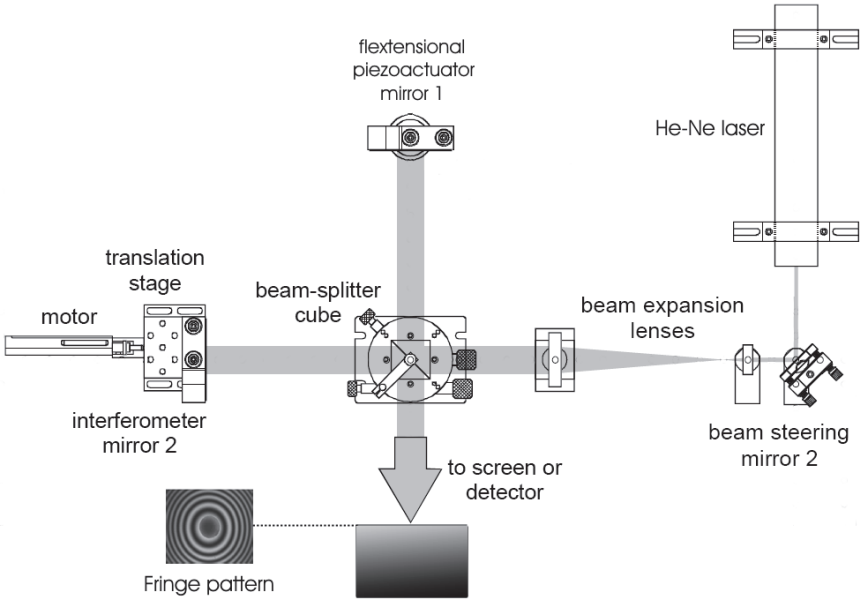


Figure 3. Homodyne Michelson interferometer used to characterize the MAPFA.

At the output of a homodyne Michelson interferometer, the photodetected voltage can be related to dynamic phase shift, $\phi(t)$, as follows (Udd and Spillman, 2011):

$$v(t) = \frac{I}{2}\{1 + F\cos[\phi_0(t) + \phi(t)]\}, \tag{1}$$

where $I$ is a proportionality constant that depends on the optical source intensity, the photodetector responsivity and the signal conditioning circuit gain. Factor $F$ is related to the interference fringe visibility and $\phi_0(t)$ is a static phase (in principle). The phase $\phi_0(t)$ should ideally remain constant, but in practice it is susceptible to signal fading, i.e., low frequency fluctuations in the local temperature of the interferometer, external mechanical vibrations, and air turbulence, that produce differential drifts on the interferometer arms, causing large phase shifts in $\phi_0(t)$ (Sheem et al., 1982). Consequently, random variations in the amplitude of the photodetected signal occur, severely limiting the direct

applicability of the sensor system. For this reason, adequate techniques must be applied to obtain a linear relationship between the output electrical signal and induced phase-shift.

When a piezoactuator is excited with a sinusoidal voltage $V(t) = V_{\text{peak}} \sin(\omega_s t)$, with amplitude $V_{\text{peak}}$ and angular frequency $\omega_s$, the signal phase-shift between the sensor and reference beams in the interferometer can be written as follows (Udd and Spillman, 2011):

$$\phi(t) = x \sin(\omega_s t), \tag{2}$$

where $x$ is the modulation index or amplitude of the phase change. By detecting the light intensity at the interferometer output, the electric voltage can be estimated from (Sudarshanam and Srinivasan, 1989):

$$v(t) = A + B\{\cos\phi_0(t)[J_0(x) + 2J_2(x)\cos 2\omega_s t + ...] - \sin\phi_0(t)[2J_1(x)\sin\omega_s t + 2J_3(x)\sin 3\omega_s t + ...]\}, \tag{3}$$

where $A$ and $B$ are constants, and the terms $J_m(x)$ are Bessel functions of the first kind and order $m$. Once $x$ is determined, the piezoactuator vibration amplitude or surface displacement at the measurement point is given by (Udd and Spillman, 2011):

$$\Delta u = \lambda\, x / 4\pi \tag{4}$$

where $\lambda$ is the light wavelength. The interferometry problem is posed as the detection of very low values of modulation index $x$ under high values of random phase shift $\phi_0(t)$ and under the presence of electronic noise.

Methods of spectrum analysis of the interferometer output can be used to measure displacements by simple passive phase-detection schemes, independently of fading (Deferrari et al., 1967; Sheem et al., 1982; Sudarshanam and Srinivasan, 1989; Udd and Spillman, 2011). Dynamic phase demodulation methods using spectral analysis techniques are classic tools used since the 1920's (Thomas and Warren, 1928), that were established and evolved significantly after the 1960's, with the advent of the laser. For example, the $J_1/J_3$ method was proposed in the classic article of Deferrari et al. (1967), together with other methods like the $J_1/J_2$ and $J_1max$. Nevertheless, some drawbacks or misunderstandings about some of these methods usually are not pointed out in the literature.

In order to understand the $J_1/J_3$ method, consider the even and odd harmonic amplitudes of $v(t)$ in Eq. (3):

$$V_{2n} = 2BQJ_{2n}(x) \text{ and } V_{2n-1} = 2BPJ_{2n-1}(x) \tag{5}$$

respectively, and $n = 1, 2, 3, \ldots$, where $P = \sin\phi_0(t)$ and $Q = \cos\phi_0(t)$. For example, the well known $J_1/J_3$ method uses the fundamental ($V_1$) and third ($V_3$) harmonics of the interferometric signal and calculates the ratio $V_1/V_3 = J_1(x)/J_3(x)$. In this operation only the odd spectral components are involved and, consequently, the amplitude factors associated to $V_1$ and $V_3$, related to intensity of the optical sources, photodetector responsivity and fringe visibility, are cancelled and the computation of $x$ does not depend on $\phi_0(t)$. As a result, the $J_1/J_3$ method is immune to fading and does not depend on the values or instabilities in the amplitude factors.

However, there are some troubles with the $J_1/J_3$ technique such as the difficulty to solve a transcendental equation and the phase ambiguity problem. Actually, for a given $V_1/V_3$ ratio there are infinite solutions for $x$, due to the oscillatory behaviour of the Bessel functions $J_n(x)$. This characteristic restricts the application of the method to those cases when $x$ increases from zero, in order to track the evolution of the transcendental equation solution. Another problem refers to the algebraic sign of the Bessel functions (as an example, for $x$>3.83 rad, $J_1(x)$ becomes negative for the first time), that must be considered when using the magnitude factors. Furthermore, Deferrari et al. (1967) did not take into account the electronic noise in the photodetection method, which varies the SNR concomitantly with the variation of $\phi_0(t)$. Then, depending on the value of $x$, $\phi_0(t)$ and order $n$, the magnitudes of $V_1$ and (principally) $V_3$ can present the same order of magnitude of noise, or even less. According to Sudarshanam (1992) the *MDPS* (Minimum Detectable Phase Shift) is the value of $x$ that satisfies the condition $\Delta x = x$ (in analogy to the signal-to-noise ratio, SNR), where $\Delta x = |x' - x|$ is the absolute error between the estimated value $x'$ and the expected value $x$ of the modulation index, in the presence of noise. For the $J_1/J_3$ method and considering $1/f^2$ power noise (red noise), the *MDPS* is 0.18 rad. Below this value, noise predominates (over the component $V_3$) and the estimated value of $x$ diverges 100% from the expected value. Consequently, the $J_1/J_3$ method does not operate for small values of $x$.

In this work, a new and improved version of the $J_1/J_3$ method is proposed, which overcomes most of the limitations cited previously.

## 4. THE GENERALIZED $J_1/J_3$ INTERFEROMETRIC METHOD

In this work, an improved version of the $J_1/J_3$ method is proposed, which is here denominated "generalized $J_1/J_3$ method". The objective is to establish a standard and computationally simple procedure to estimate values of $x$ as high as 130 rad (or higher). The challenge is to do it when there is fading, which is manifested by the low frequency random phase $\phi_0(t)$. The first step is to determine the magnitude spectrum of the photodetected signal in Eq. (1), as given by Eq. (3). Figure 4 shows a typical a.c. instantaneous waveform and the corresponding Fourier spectrum presented at the interferometer output, like that shown in Fig. 3, where $V_1$, $V_2$, $V_3$, etc., are the voltage magnitudes of the fundamental and the higher order harmonics. The $J_1/J_3$ generalized computational algorithm is based on the value of $n=f_n/f_0$, where $f_n$ is the frequency corresponding to higher magnitude and $f_0$ is the fundamental frequency of the MAPFA drive voltage (in Fig. 4, $n$=9).

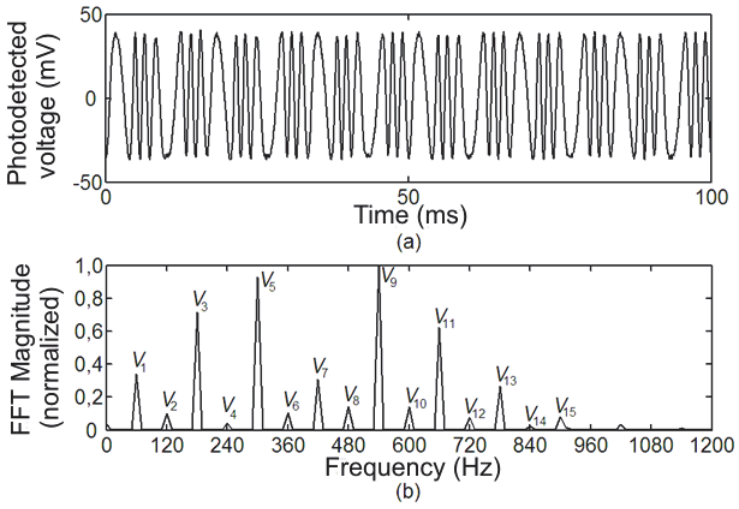


Figure 4. Typical output interferometric signal observed when the MAPFA is driven with a sinusoidal voltage. a) Photodetected signal. b) The corresponding spectrum

The determination of the modulation index $x$ is performed using software Matlab, more specifically, the fzero command, which tries to find a zero of a certain function $f(x)$ near $x_0$, if $x_0$ is a scalar (Attaway, 2011). However, two ranges of values of $n$ must be tested: $n \geq 3$ and $n < 3$. Basically, if $n \geq 3$ the algorithm involves two steps:

**Step1:** Obtain, as a first approximation for $x$, named as $x_0$, the value of $x$ where the difference:

$$d(x) = \left\{ \frac{|J_n(x)|}{|J_{n+2}(x)|} - \frac{|V_n|}{|V_{n+2}|} \right\} \tag{6}$$

becomes minimum within the range between $x_{min}$ and $x_{max}$, where $x_{min}$ is the first point of intersection between the functions $J_{n-2}(x)$ and $J_n(x)$, and $x_{max}$ is the first point of intersection between $J_n(x)$ and $J_{n+2}(x)$;

**Step 2:** Given $x_0$ obtained in Step 1, use the fzero command to find the root of the function $f(x')$, such as:

$$f(x') = \left\{ \frac{|J_n(x')|}{|J_{n+2}(x')|} - \frac{|V_n|}{|V_{n+2}|} \right\} \tag{7}$$

near the value of $x_0$ found in Step 1, where $x'$ is the estimated (or measured) modulation index and $x$ is the expected value of the modulation index.

However, if $n < 3$, ambiguity cases occur when the harmonic with $n$ = 1 or $n$ = 2 becomes maximum for the second time when $x$ increases, depending on the value of random phase shift $\phi_0(t)$.

Actually, an important detail resides in the envelope of maxima and the corresponding value of $n$, as $x$ increases. As there is interest in the maximum magnitude for each value of $x$ consider, for example, the particular case where $\phi_0 = \pi/2$ rad. First, there is a region where $V_1(x)$ (given by Eq. (5)) is maximum, for $0 \leq x \leq 3.0558$ rad; then $V_3(x)$ is maximum from 3.0558 to 5.1363 rad; then $V_1(x)$ is maximum again, from 5.1363 to 5.6164; then $V_5(x)$, for $5.6164 \leq x \leq 7.5019$ rad. The authors have observed that for higher values of $x$ after this point, the sequence of maxima are related to functions $V_7(x)$, $V_9(x)$, $V_{11}(x)$, etc. This was verified up to 130 rad, but is possibly valid until infinity. Consequently,

there is only one ambiguity, related to function $V_1(x)$, which is maximum at two disjoint intervals. The challenge is to realize a similar analysis when there is fading, which is manifested by low frequency and time varying random phase $\phi_0(t)$. However, it can be shown that same conclusion are obtained for values of $\phi_0(t)$ in the range $\pi/2 - 0.3156\pi \leq \phi_0(t) \leq \pi/2 + 0.3156\pi$ and $3\pi/2 - 0.3156\pi \leq \phi_0(t) \leq 3\pi/2 + 0.3156\pi$ rad.

On the other hand, for the particular case where $\phi_0 = \pi$ rad, the even harmonics are higher than the odd ones, and increasing values of $x$, the harmonic with order $n = 2$ is larger, then $n = 4$, then again $n = 2$, then $n = 6$, and so on. The same conclusion is obtained for values of $\phi_0(t)$ in the range $-0.1974\pi \leq \phi_0(t) \leq 0.1974\pi$ and $\pi - 0.1974\pi \leq \phi_0(t) \leq \pi + 0.1974\pi$ rad.

Finally, a detailed analysis for the remaining values of $\phi_0(t)$ reveals that the ambiguity cases (when harmonic with $n = 1$ or $n = 2$ become maximum for the second time) do not occur.

Thus, in the case for $n < 3$, the authors found out that the ratio $|V_{n+4}|/|V_n|$ must be calculated. If $|V_{n+4}|/|V_n| < 0.6$, then this corresponds to the standard case. Consequently, the value of $n$ should be maintained and Steps 1 and 2 should be applied. Otherwise, if $|V_{n+4}|/|V_n| > 0.6$, then the value of $n$ is replaced by ($n$ +2) and Steps 1 and 2 should be applied to this new value of $n$. This is the treatment for the ambiguity case. However, it must be adopted $x_{min}=0^+$ (or $x_{min}$=eps in Matlab) for both, $n$=1 and $n$=2; the value of $x_{max}$ remains the same, i.e., the first intercept between $J_n(x)$ and $J_{n+2}(x)$.

An important advantage of the method is that there is no problems with singularities of the type $\phi_0(t) = \ell\pi/2$ rad for $\ell = \pm1, \pm2, \pm3, \ldots$, and it is not necessary to use any algorithm to detect Bessel function algebraic sign inversion, as occurs with the modified $J_1...J_4$ method (Jin et al., 1991). This is valid for any value of $x$ larger than the *MDPS*, which was verified in this work up to 130 rad.

The proof of the $J_1/J_3$ algorithm is too long to be presented here and it will be submitted for publishing in a regular paper.

## 5. EXPERIMENTAL RESULTS

MAPFA displacements are measured by using a low cost open loop homodyne bulk Michelson interferometer, where a He-Ne laser source (Newport, 15 mW, $\lambda$ = 632.8 nm) and a PIN photodiode (ThorLabs, PDA 55) are used. The output signal was digitized by an oscilloscope (Tektronix TDS2022) and transferred to a computer to be post processed. A commercially available reflective sheet (3M Scotch-lite 7610) covered with 60 μm diameter spherical glass lenses are mounted on the surface of the sample (3M Scotchlite, 2003). The input sinusoidal voltage amplitude is varied from 0 to 180 V (peak) and the linearity curves of the MAPFA are obtained. Output signal like that shown in Fig. 4 are obtained, and the corresponding spectra are determined. The modulation index $x$ is obtained from the generalized $J_1/J_3$ method, and displacements are calculated by applying Eq. (4). Displacements are determined by considering low excitation frequencies.

The results for generated displacements at the frequencies of 370 Hz, 930 Hz and 2.811 kHz are presented in Fig. 5. As can be seen, the generalized $J_1/J_3$ method reaches 130 rad (650 nm). There is a linear response starting from 0.18 rad, and the PFA linear length-to-voltage sensitivities resulted in 0.2684, 0.4102 and 0.8613 nm/V (peak), at the frequencies of 370 Hz, 930 Hz and 2.811 kHz, respectively.

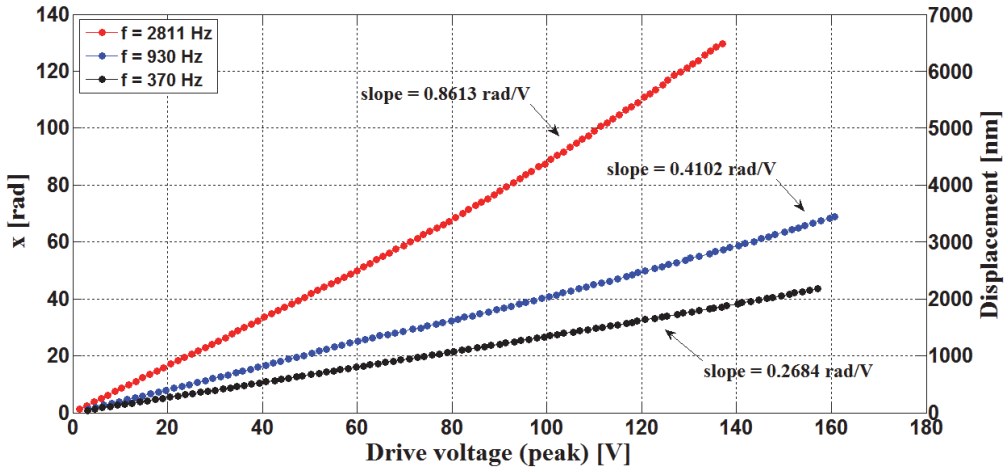


Figure 5. XY nanopositioner generated movement linearity curves at the frequencies of 370 Hz, 930 Hz and 2,811 Hz.

In Fig. 6 the results for coupled displacements at the frequencies of 290 Hz, 910 Hz and 1.25 kHz are presented. The displacement amplitudes in Fig. 5 are smaller than those shown in Fig. 4 for the corresponding voltages. There is a linear response starting from 0.18 rad, and the MAPFA linear length-to-voltage sensitivities resulted in 0.05806, 0.21924 and 1.1003 nm/V (peak), at the frequencies of 290 Hz, 910 Hz and 1.25 kHz, respectively.

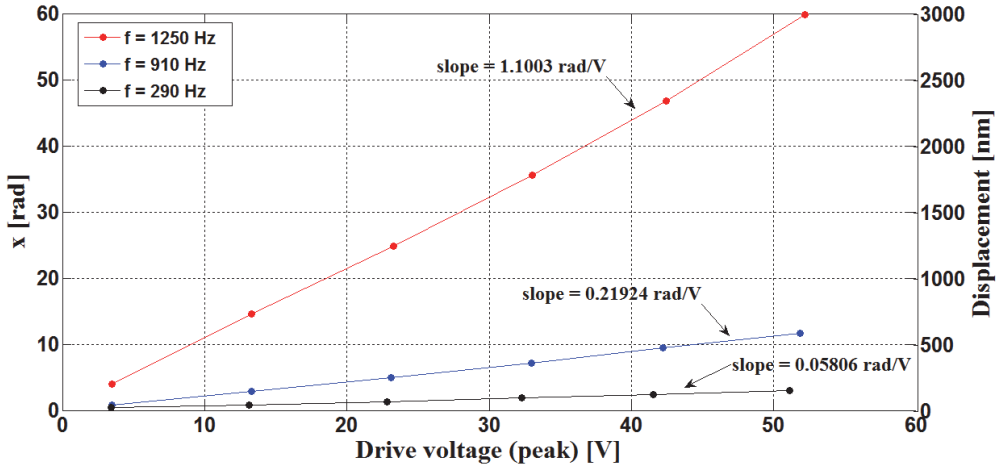


Figure 6. XY nanopositioner coupled movement linearity curves at the frequencies of 290 Hz, 910 Hz and 1,250 Hz.

The frequency response shows the MAPFA mechanical resonance frequencies, as well as the quasi-static range of operation. The frequency response, in terms of the modulation index- and length-to-voltage ratios, is presented in Fig. 7 (in terms of mean and standard deviation), for frequencies between 76 Hz and 4 kHz. There are mechanical resonances at the frequencies of 956 Hz, 1.18 kHz, 1.24 kHz, 1.39 Hz and 2.96 kHz in the studied range. At 370 Hz, 930 Hz and 2.811 kHz there was agreement with the linearity responses (slope, in terms of modulation index- and length-to-voltage ratios) from Fig. 5 and Fig. 6. The PFA –3 dB operation bandwidth is approximately 895 Hz.

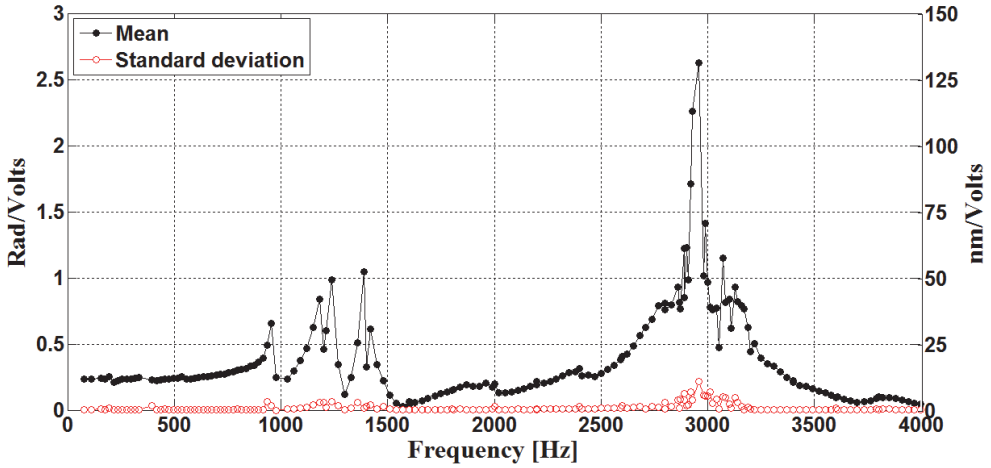


Figure 7. Generated XY nanopositioner displacement frequency response, in terms of modulation index- and length-to-voltage ratios.

The MAPFA coupled movement frequency response is shown in Fig. 8, for frequencies between 90 Hz and 1.27 kHz. There are resonances around 370 Hz, 990 Hz, 1,170 Hz, and 1,250 Hz in the studied range. It is observed that near these frequencies the coupled displacement have similar amplitudes as the generated movements. This means that this XY nanopositioner would not be useful when operating at resonances.

A quantitative measure of the crosstalk levels between X and Y displacements can be given in terms of percentage by the following expression (Carbonari et al., 2005b):

$$S_{xy} = \Delta y_s / \Delta x \tag{8}$$

where $\Delta x$ is the desired displacement in the X direction and $\Delta y_s$ is the spurious displacement found in Y direction when attempt to displace in X. From the data of generated and coupled movements (Fig. 7 and Fig. 8), the coupling rate $S_{xy}$ defined in Eq. (8) can be measured as a function of frequency. The result is shown in Fig. 9.

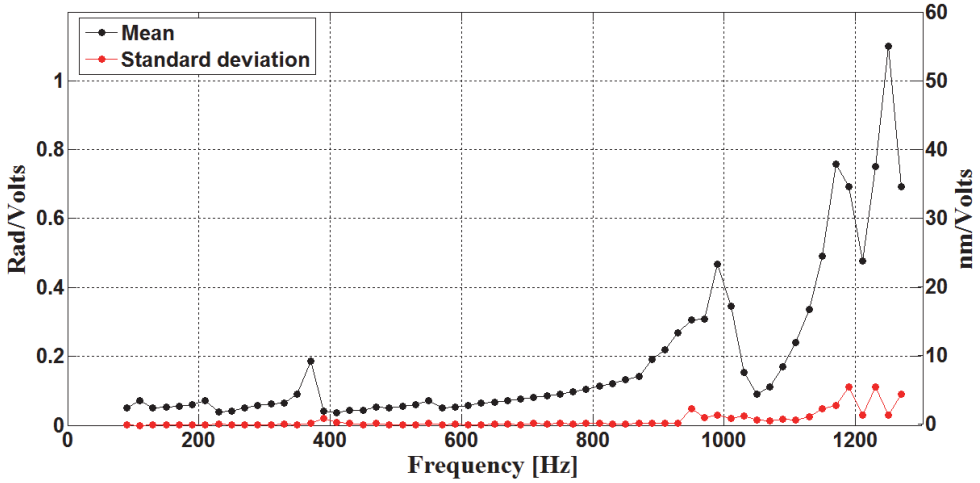


Figure 8. Coupled XY nanopositioner displacement frequency response, in terms of modulation index- and length-to-voltage ratio.

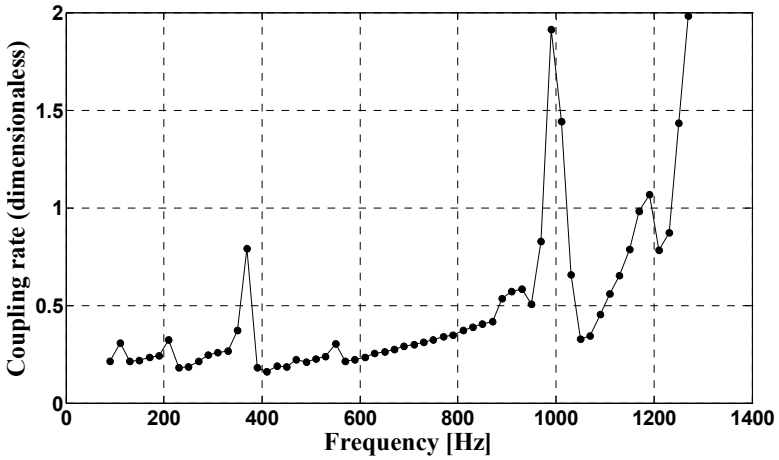


Figure 9. Coupling rate $S_{xy}$ as a function of frequency.

## 6. CONCLUSIONS

Modulation indexes values up to 130 rad can be measured with high accuracy by using the new generalized $J_1/J_3$ method. This range is sufficient to analyze the MAPFAs discussed in section 2. However, it is important to emphasize that this limit can increase indefinitely, being limited only by the detector and data acquisition frequency bandwidths employed.

In Precision Engineering, the precision degree is related to the ratio between the resolution/uncertainty range, defined as precision ratio (*PR*) by Fan et al. (2007). As it was shown, the generalized $J_1/J_3$ method proposed here allows to obtain one of the best *PR* values using homodyne interferometers: *PR* equal $1.1 \times 10^{-3}$ (range between 10 nm and 8.7 μm). Better values are obtained than those obtained by most successful homodyne systems such as, for example, Jin et al. (1992), with $PR = 3.8 \times 10^{-3}$, and Ivaschescu (2000), with $PR = 6.3 \times 10^{-3}$. On the other hand, it presents a *PR* worse than that obtained by (Heinzel et al., 2010), applied to the detection of gravitational waves: $PR = 10^{-5}$. In the case of that article, however, the interest has been focused on expanding the dynamic range by improving resolution, operating from 20 pm to 1 μm, approximately.

Finally, it is noteworthy that the range presented in this work (from 10 nm to 8.7 μm), although it cannot be expanded to improve the resolution, in principle, can be easily expanded up to unlimited amounts, since is provided

with a detection system, and data acquisition bandwidth higher than used herein. So, it is important to clarify that the not so high value of *PR* obtained here is due to technological limitations of the experimental setup.

The coupling factor was calculated, showing its frequency dependence, and concluding that, when the XY nanopositioner is in resonance, the whole structure vibrates, and the generated and coupled displacements are of the same order of magnitude. Under this condition the MAPFA operation is impracticable.

## 7. ACKNOWLEDGEMENTS

The authors are grateful to the research agencies FAPESP (project number 2012/01629-7), CNPq (project number 478817/2012-6) and CAPES in Brazil.

## 8. REFERENCES

Attaway, S., 2011. *MATLAB - A Fundamental Tool for Scientific Computing and Engineering Applications*, Vol. 1, 2nd ed., InTech, Janeza Trdine, Croatia.

Brand, U. and Herrmann, K., 1996. "A laser measurement system for the high-precision calibration of displacement transducers". *Measurement Science and Technology*, Vol. 7, p. 911.

Carbonari, R. C., Silva, E. C. N., and Nishiwaki, S., 2005a. "Design of piezoelectric multi-actuated microtools using topology optimization". *Smart Materials and Structures*, Vol.14, p.1431.

Carbonari, R. C., Nader, G., Nishiwaki, S., and Silva, E. C. N., 2005b. "Experimental and numerical characterization of multi-actuated piezoelectric device designs using topology optimization". In *Proceedings of SPIE. Vol. 5764*, San Diego, CA, USA.

Carbonari, R. C., Silva, E. C. N., and Nishiwaki, S., 2007. "Optimum placement of piezoelectric material in piezoactuator design". *Smart Materials and Structures*, Vol.16, p.207.

Carbonari, R. C., Silva, E. C. N., and Paulino, G. H., 2009. "Multi-actuated functionally graded piezoelectric micro-tools design: A multiphysics topology optimization approach". *International Journal for Numerical Methods in Engineering*, Vol. 77, p. 301.

Chassagne, L., Blaize, S., Ruaux, P., Topu, S., Royer, P., Alayli, Y., and Lrondel, G., 2010. "Note: multiscale scanning probe microscope". *Rev. Sci. Instrum*, Vol. 81, p. 086101.

Cherepanov, V., Coenen, P., and Voigtländer, B., 2012. "A nanopositioner for scanning probe microscopy: The koaladrive". *Review of Scientific Instruments*, Vol. 83, p. 023703.

Deferrari, H. A., Darby, R. A., and Andrews, F. A., 1967. "Vibrational displacement and mode-shape measurement by a laser interferometer", *J. Acoust. Soc. Am.*, Vol. 42, p. 982.

Devasia, S., Eleftheriou, E., and Moheimani, S., 2007. "A survey of control issues in nanopositioning". *IEEE Transactions on Control Systems Technology*, Vol. 15, p. 802.

Fan, K.-C., Lai, Z.-F., Wu, P., Chen, Y.-C., Chen, Y., and Jäger, G., 2007. "A displacement spindle in a micro/nano level". *Measurement Science and Technology*, Vol. 18, p. 1710.

Heinzel, G., Cervanyes, F. G., Marin, A. F. G., Kullmann, J., Feng, W., and Danzmann, K., 2010. "Deep phase modulation interferometry". *Optics Express*, Vol. 18, p. 19076.

Hausotte, T., Percle, B., Gerhardt, U., Dontsov, D., Manske, E. , and Jäger, G., 2012. "Interference signal demodulation for nanopositioning and nanomeasuring machines". *Measurement Science and Technology*, Vol. 23, p. 074004.

Ivaschescu, V., 2000. "Small sinusoidal vibrations amplitude measurements with the Michelson interferometer". *IEEE Transactions on Instrumentation and Measurement*, Vol. 49, p. 643.

Jin, W., Zhang, L. M., Uttamchandani, D., and Cuishaw, B., 1991. "Modified $J_1...J_4$ method for linear readout of dynamic phase changes in a fiber-optic homodyne interferometer", *Applied Optics*, Vol. 30, p. 4496.

Jin, W., Uttamchandani, D., and Culshaw, B., 1992. "Direct readout of dynamic phase changes in a fiber-optic homodyne interferometer". *Applied Optics*, Vol. 31, p. 7253.

Kuo, S.-K., Hung, C.-C., Lin, C.-C., and Yang, W.-H., 2007. "Development of a nanodisplacement measurement system". *Measurement*, Vol. 40, p.255.

Novikov, Y. A., Ozerin, Y. V., Rakov, A. V., and Todua, P. A., 2007. "Method for linear measurements in the nanometre range". *Measurement Science and Technology*, Vol. 18, p. 367.

Schibli, T. R., Minoshima, K., Bitou, Y., Hong, F.-L., Inaba, H., Onae, A., and Matsumoto, H., 2006. "Displacement metrology with sub-pm resolution in air based on a fs-comb wavelength synthesizer". *Optics Express*, Vol. 14, p. 5984.

Sheem, S. K., Giallorenzi, T. G., and Koo, K., 1982. "Optical techniques to solve the signal fading problem in fiber interferometers". *Applied Optics*, Vol. 21, p. 689–693.

Shi, H., Su, H.-J., Dagalakis, N., and Kramar, J. A., 2013. "Kinematic modeling and calibration of a flexure based hexapod nanopositioner". *Precision Engineering*, Vol. 37, p. 117.

Smith, D. T., Pratt, J. R., and Howard, L. P., 2009. "A fiber-optic interferometer with subpicometer resolution for dc and low-frequency displacement measurement". *Review of Scientific Instruments*, Vol. 80, p. 035105.

Sudarshanam, V. S. and Srinivasan, K., 1989. "Linear readout of dynamic phase change in a fiber-optic homodyne interferometer". *Optics Letters*, Vol 14, p. 140–142.

Sudarshanam, V. S., 1992. "Minimum detectable phase shift in spectrum-analysis techniques of optical interferometric vibration detection". *Applied Optics*, Vol. 31, p. 5997.

Thomas, H. A. and Warren, G. W., 1928. "An optical method of measuring small vibrations", *Phil. Mag*., Vol. 5, p. 1125.

Tian, Y., Shirinzadeh, B., and Zhang, D., 2009. "A flexure-based five-bar mechanism for micro/nano manipulation". *Sensors and Actuators A: Physical*, Vol. 153, p. 96.

3M Scotchlite, "High gain reflective sheeting 7610 - Technical Data". May 2003, <http://solutions.3m.com/wps/portal/3M/en_US/ Manufacturing/Industry/Product-Catalog/Online-Catalog>, Accessed in May 2013.

Udd, E. and Spillman, W. B. J., 2011. *Fiber Optic Sensors: An Introduction for Engineers and Scientists*. Wiley, New York.

Zhelkobaev, Zh., Kalendin, V. V., Samorukov, M. A., and Todua, P. A., 2007. "Laser interferometry-phasometry of nanodisplacement" *In Proceedings of SPIE Vol. 6594*, Moscow, Russia.

## 9. RESPONSIBILITY NOTICE

The authors are the only responsible for the printed material included in this paper.